Cellular/Molecular

Protein Kinase C and Calmodulin Serve As Calcium Sensors for Calcium-Stimulated Endocytosis at Synapses

Ying-Hui Jin,[1,2]* Xin-Sheng Wu,[1]* Bo Shi,[1,3]* Zhen Zhang,[1] Xiaoli Guo,[1] Lin Gan,[4] Zhongqing Chen,[2] and Ling-Gang Wu[1]

[1]National Institute of Neurological Disorders and Stroke, Bethesda, Maryland 20892, [2]Department of Critical Care Medicine, Nanfang Hospital, Southern Medical University, Guangzhou, China 510515, [3]Biological Sciences Graduate Program, College of Computer, Mathematical, and Natural Sciences, University of Maryland, College Park, Maryland 20740, and [4]Flaum Eye Institute, University of Rochester School of Medicine and Dentistry, Rochester, New York 14642

Calcium influx triggers and facilitates endocytosis, which recycles vesicles and thus sustains synaptic transmission. Despite decades of studies, the underlying calcium sensor remained not well understood. Here, we examined two calcium binding proteins, protein kinase C (PKC) and calmodulin. Whether PKC is involved in endocytosis was unclear; whether calmodulin acts as a calcium sensor for endocytosis was neither clear, although calmodulin involvement in endocytosis had been suggested. We generated PKC (α or β-isoform) and calmodulin (calmodulin 2 gene) knock-out mice of either sex and measured endocytosis with capacitance measurements, pHluorin imaging and electron microscopy. We found that these knock-outs inhibited slow (~10–30 s) and rapid (<~3 s) endocytosis at large calyx-type calyces, and inhibited slow endocytosis and bulk endocytosis (forming large endosome-like structures) at small conventional hippocampal synapses, suggesting the involvement of PKC and calmodulin in three most common forms of endocytosis-the slow, rapid and bulk endocytosis. Inhibition of slow endocytosis in PKC or calmodulin 2 knock-out hippocampal synapses was rescued by overexpressing wild-type PKC or calmodulin, but not calcium-binding-deficient PKC or calmodulin mutant, respectively, suggesting that calcium stimulates endocytosis by binding with its calcium sensor PKC and calmodulin. PKC and calmodulin 2 knock-out inhibited calcium-dependent vesicle mobilization to the readily releasable pool, suggesting that PKC and calmodulin may mediate calcium-dependent facilitation of vesicle mobilization. These findings shed light on the molecular signaling link among calcium, endocytosis and vesicle mobilization that are crucial in maintaining synaptic transmission and neuronal network activity.

Key words: **calmodulin; capacitance measurement; electron microscopy; endocytosis; pHluorin imaging; protein kinase C**

Significance Statement

Vesicle fusion releases neurotransmitters to mediate synaptic transmission. To sustain synaptic transmission, fused vesicles must be retrieved via endocytosis. Accumulating evidence suggests that calcium influx triggers synaptic vesicle endocytosis. However, how calcium triggers endocytosis is not well understood. Using genetic tools together with capacitance measurements, optical imaging and electron microscopy, we identified two calcium sensors, including protein kinase C (α and β isoforms) and calmodulin, for the most commonly observed forms of endocytosis: slow, rapid, and bulk. We also found that these two proteins are involved in calcium-dependent vesicle mobilization to the readily releasable pool. These results provide the molecular signaling link among calcium, endocytosis, and vesicle mobilization that are essential in sustaining synaptic transmission and neuronal network activity.

Introduction

Endocytosis mediates fundamental functions, such as vesicle recycling to sustain synaptic transmission, intracellular trafficking of proteins and lipids vital for every cell, and viral entry (L.G. Wu et al., 2014; Kononenko and Haucke, 2015). Two sets of evidence

Received Jan. 15, 2019; revised Aug. 27, 2019; accepted Oct. 7, 2019.

Author contributions: Y.-H.J., X.-S.W., B.S., L.G., Z.C., and L.-G.W. designed research; Y.-H.J., X.-S.W., B.S., Z.Z., and X.G. performed research; Y.-H.J., X.-S.W., B.S., and Z.Z. analyzed data; B.S. and L.-G.W. edited the paper; L.G. and Z.C. contributed unpublished reagents/analytic tools; L.-G.W. wrote the first draft of the paper; L.-G.W. wrote the paper.

This work was supported by the National Institutes of Health (NIH)–National Institute of Neurological Disorders and Stroke Intramural Research Program. Y.-H.J. is in the individual graduate partnership program between NIH and Southern Medical University, Guangzhou, China. We thank Yongling Zhu for providing SypH plasmid and Susan Cheng, Virginia Crocker, and Sandra Lara for EM technical support.

The authors declare no competing financial interests.

*Y.-H.J, X.-S.W., and B.S. contributed equally to this work.

Z. Zhang's present address: Office of Genetic Drugs, Center for Drug Evaluation and Research, Food and Drug Administration, 10903 New Hampshire Ave., Silver Spring, MD 20993.

Correspondence should be addressed to Ling-Gang Wu at wul@ninds.nih.gov.

https://doi.org/10.1523/JNEUROSCI.0182-19.2019

at calyx of Held synapses suggest that calcium triggers slow endocytosis (>10 s), rapid endocytosis (<~3 s), bulk endocytosis (retrieving endosome-like structures larger than regular vesicles), and endocytosis overshoot (more endocytosis than exocytosis) (Hosoi et al., 2009; Wu et al., 2009; Yamashita et al., 2010; for review, see L.G. Wu et al., 2014). First, lowering extracellular calcium or buffering calcium with BAPTA reduces the rate of rapid and slow endocytosis by ~50 to 1500 fold and abolishes endocytosis overshoot, whereas increasing calcium current charges increases endocytosis rate by hundreds of folds and promotes endocytosis overshoot. Second, calcium chelator EGTA inhibits bulk endocytosis and reduces the fission pore closure rate. Consistent with these results, calcium influx triggers rapid endocytosis at chromaffin cells (Artalejo et al., 1995; Chiang et al., 2014) and slow endocytosis at hippocampal synapses (Sun et al., 2010); calcium influx upregulates rapid, slow, bulk, and/or overshoot endocytosis at hippocampal synapses, retinal nerve terminals, hair cells, chromaffin cells and pituitary neurons (Thomas et al., 1994; Smith and Neher, 1997; Moser and Beutner, 2000; Neves et al., 2001; Sankaranarayanan and Ryan, 2001; Balaji et al., 2008; Clayton et al., 2009).

Like calcium-induced exocytosis, the first step in the study of calcium-stimulated endocytosis is to identify calcium sensor. The candidate being considered for the last two decades is calcium/calmodulin-activated calcineurin (CaN), which dephosphorylates endocytic proteins (Cousin and Robinson, 2001). Pharmacological block or knock-down of calmodulin (CaM) and knock-out of CaN led to slower endocytosis at synapses, raising the possibility that CaM and CaN serve as the calcium sensors for endocytosis (Sun et al., 2010; X.S. Wu et al., 2014; Cottrell et al., 2016). However, whether CaM or CaN involvement in endocytosis depends on their calcium binding, the condition required for establishing CaM/CaN as the calcium sensor, has not been tested.

In the present work, we attempted to identify the calcium sensor by generating mice with deletion of calcium-activated protein kinase C (PKC) α or β isoform (PKC_α or PKC_β), and calcium-activated CaM isoform 2 (CaM_2). We determined whether these knock-outs inhibit rapid, slow and bulk endocytosis at large calyceal nerve terminals and small conventional hippocampal synapses and if the inhibition can be rescued by the wild-type (WT) or the calcium-binding-deficient proteins. We found that PKC (PKC_α or PKC_β) and CaM serve as calcium sensors for calcium-stimulated slow, rapid, and bulk endocytosis at calyceal and hippocampal synapses. These findings provide the molecular link between the calcium trigger and endocytosis mediation at synapses: PKC-mediated phosphorylation and CaM/CaN-mediated dephosphorylation.

Materials and Methods

Animals. Animal care and use were performed according to National Institutes of Health (NIH) guidelines and were approved by the NIH Animal Care and Use Committee. $PKC_\alpha^{+/-}$ mice were purchased from The Jackson Laboratory; $PKC_\beta^{-/-}$ and $CaM_2^{-/-}$ mice were generated by us, as described in detail in the legends to Figures 1*A* and 6*A*. Knock-out mice of either sex were obtained by heterozygous and homozygous breeding using standard mouse husbandry procedures. Mouse genotypes were determined by PCR. WT littermates and WT nonlittermates of either sex were used as controls.

Slice preparation, capacitance recordings, and solutions. Parasagittal brainstem slices (200 μm thick) containing the medial nucleus of the trapezoid body were prepared from 7- to 14-d-old male or female mice using a vibratome (Wu et al., 2009). Whole-cell capacitance measurements were made with the EPC-9 amplifier with a software lock-in amplifier (1000 Hz sine wave, peak-to-peak voltage ≤ 60 mV; HEKA). We pharmacologically isolated presynaptic Ca^{2+} currents with a bath solution (~22–24°C or 34–37°C when mentioned) containing the following (in mM): 105 NaCl, 20 TEA-Cl, 2.5 KCl, 1 $MgCl_2$, 2 $CaCl_2$, 25 $NaHCO_3$, 1.25 NaH_2PO_4, 25 glucose, 0.4 ascorbic acid, 3 *myo*-inositol, 2 sodium pyruvate, 0.001 tetrodotoxin (TTX), 0.1 3,4-diaminopyridine, pH 7.4 when bubbled with 95% O_2 and 5% CO_2. The presynaptic pipette contained the following (in mM): 125 Cs-gluconate, 20 CsCl, 4 MgATP, 10 Na_2-phosphocreatine, 0.3 GTP, 10 HEPES, 0.05 BAPTA, pH 7.2, adjusted with CsOH. If not mentioned otherwise, all reagents were from Sigma-Aldrich. Bisindolylmaleimide I (BIS) was from Calbiochem.

In experiments with temperature changes, the continuously flowing solution reached the slice chamber via a tube, which was heated to ~40–42°C right (at ~10–15 cm) before the solution reached the chamber. With a flow rate of ~2.5 ml/min, the chamber temperature was maintained at 34–37°C, as confirmed with a thermometer. Slices were at 34–37°C for ~15–20 min before patching.

Hippocampal culture. Mouse hippocampal culture was prepared as described previously (Sankaranarayanan and Ryan, 2000; Sun et al., 2010). Hippocampal CA1-CA3 regions from P0 mice were dissected, dissociated, and plated on Poly-D-lysine-treated coverslips. Cells were maintained at 37°C in a 5% CO_2 humidified incubator with a culture medium consisting of Neurobasal A (Invitrogen), 10% fetal bovine serum (Invitrogen), 2% B-27 (Invitrogen), 1% Glutamax-1 (Invitrogen). On 5–7 d after plating, neurons were transfected with plasmids using Lipofectamine LTX (Invitrogen).

Hippocampal cultures were transfected with a plasmid containing synaptophysin tagged with the pH-sensitive pHluorin2X (SypH, provided by Dr. Yong-Ling Zhu) (Zhu et al., 2009) for imaging of endocytosis. cDNA encoding human PKC_α WT was amplified from pHACE-PKC_α (Addgene, 21232) and subcloned into PmCherry-N1 (Clontech) (mCherry used for recognition of transfection). Mutant $PKC_\alpha^{D/A}$ was generated by replacing the five aspartates in the calcium binding C2 domain (Nalefski and Falke, 1996) with alanines through site-directed mutagenesis (QuikChange Lightning; Agilent Technologies). Similar to WT PKC_α, $PKC_\alpha^{D/A}$ was subcloned into PmCherry-N1.

The cDNA encoding CaM or CaM_{1234}, provided by the late Dr. David Yue, was subcloned into PmCherry-N1. For PKC or CaM rescue experiments (see Figs. 4; 7), we transfected PKC or CaM plasmid along with SypH. PKC or CaM plasmid contained mCherry, which was used for us to recognize transfected cells. After transfection, neurons were maintained at 37°C in a 5% CO_2-humidified incubator for another 8–12 d before experiments.

Action potential was evoked by a 1 ms pulse (20 mA) through a platinum electrode. The bath solution contained the following (in mM): 119 NaCl, 2.5 KCl, 2 $CaCl_2$, 2 $MgCl_2$, 25 HEPES, 30 glucose, 0.01 6-cyano-7-nitroquinoxaline-2, 3-dione (CNQX), and 0.05 D,L-2-amino-5-phosphonovaleric acid (AP-5), pH 7.4 , adjusted with NaOH. In temperature experiments, we heated the culture chamber using a temperature controller (TC344B; Warner Instruments, Hamden, CT). Imaging was performed after the culture was at 34–37°C for 15–30 min. The temperature was verified with another small thermometer (BAT-7001H; Physitemp Instruments) in the chamber. SypH images were acquired at 1 Hz using Nikon A1 confocal microscope (60×, 1.4 numerical aperture [NA]), and analyzed with Nikon software.

Immunohistochemistry and Western blot. For immunohistochemistry, P7–P10 mice were anesthetized using Nembutal and transcardially perfused with 4% paraformaldehyde (Electron Microscopy Sciences). The brain was postfixed in 4% paraformaldehyde overnight and infiltrated with 30% sucrose for another 48 h. Optimal cutting temperature medium (Electron Microscopy Sciences)-embedded brain was sectioned using cryostat (Leica, CM3050S) at 30 μm thickness. Slices were treated with cold methanol at −20°C for 10 min, and target proteins at calyces were identified using a guinea pig antibody against $vGluT_1$ (1:5000; Millipore) and a rat antibody against PKC_α (1:200; Sigma-Aldrich), a rat antibody against PKC_β (Sigma-Aldrich, 1:200) (Perrin et al., 2010), or a rat antibody against CaM (1:200; Millipore) (Perrin et al., 2010). Alexa Fluor-488-conjugated donkey anti-rat antibody (1:500; Jackson ImmunoResearch Laboratories) or Alexa Fluor 568-conjugated donkey anti-guinea pig antibody (1:500; Jackson ImmunoResearch Laboratories)

were used as secondary antibodies. Images were collected by Nikon A1 confocal microscope (objective: 60×, 1.4 NA).

For Western blot, neurons were washed three times with ice-cold PBS. Cell lysates were prepared in the modified RIPA buffer containing protease inhibitors (Thermo Scientific). Equal amounts of proteins, determined by BCA protein assay (Thermo Scientific), were loaded onto SDS-PAGE gel and immunoblotted using antibodies against PKC_α (1:250; Sigma-Aldrich), PKC_β (1:250; σ), CaM (1:200, Millinpore), clathrin heavy chain (1:1000; BD Bioscience), dynamin (1:1000; BD Biosciences; recognizing all dynamin isoforms, including 1, 2, and 3) and β-actin (1:2000; Abcam).

Data collection and measurements of τ and $Rate_{decay}$. Calyx capacitance was measured within 10 min after break-in to avoid rundown (Wu et al., 2009). The time constant (τ) of the capacitance or fluorescence decay was measured from exponential fit of the decay. The initial rate of decay ($Rate_{decay}$) of capacitance at calyces was measured between 0.5 and 4 s after a 20 ms depolarization from −80 mV to +10 mV ($depol_{20ms}$) or 20 action potential-equivalent stimuli (APe, 1 ms from −80 to +7 mV) at 100 Hz that induced slow endocytosis (Xu and Wu, 2005; Wu et al., 2009, 2016). $Rate_{decay}$ was measured between 0.5 and 1.5 s after 10 $depol_{20ms}$ at 10 Hz ($depol_{20msX10}$) or 200 APe at 100 Hz that induced rapid endocytosis. The first 0.5 s trace was not used to avoid capacitance artifact contamination (Wu et al., 2005; Yamashita et al., 2005). We used $depol_{20msX10}$ to induce rapid endocytosis, because the $Rate_{decay}$ after $depol_{20msX10}$ reflected mostly (~80%) the rapid component of endocytosis (Wu et al., 2009; Sun et al., 2010). For SypH signal in hippocampal cultures, the $Rate_{decay}$ was measured from boutons' SyPH fluorescence trace in the first 4–10 s after stimulation.

Electron microscopy. Hippocampal cultures were fixed with 4% glutaraldehyde (freshly prepared, Electron microscopy sciences, Hatfield, PA) in 0.1 M Na-cacodylate buffer solution containing for at least 1 h at 22–24°C, and stored in 4°C refrigerator overnight. The next day, cultures were washed with 0.1 M cacodylate buffer, and treated with 1% OsO_4 in cacodylate buffer for 1 h on ice, and 0.25% uranyl acetate in acetate buffer at pH 5.0 overnight at 4°C, dehydrated with ethanol, and embedded in epoxy resin. Thin sections were counterstained with uranyl acetate and lead citrate then examined in a JEOL200CX TEM. Images were collected with a CCD digital camera system (XR-100; AMT) at a primary magnification of 10,000–20,000×. Synapses were selected based on the structural specialization including synaptic vesicle clustering, synaptic cleft and the postsynaptic density.

Experimental design and statistical analyses. Data are presented as means ± SEM. The statistical test used was *t* test with equal variance, although *t* test with unequal variance gave the same result. The variance was not different, because the *p*-value was much larger than 0.05 when we performed the variance test (*F* test) for data shown in Figures 2*C*, 3*C*, and 4*C*, which show the basic findings of the present work.

For capacitance measurements at calyces, each group of data were from 4–14 calyces, which were from 4–14 mice of either sex (see figure legends for the number of calyces and mice for each group of data). For pHluorin imaging, each experiment included 20–30 boutons showing fluorescence increase (region of interest: 2 μm × 2 μm). Approximately one to three experiments were taken from each culture. Each culture was from 3–5 mice. Each group of data was obtained from at least four batches of cultures (4–12 cultures). For electron microscopy, synapses were selected based on the structural specialization, including synaptic vesicle clustering, synaptic cleft, and the postsynaptic density. Each group of data was taken from 100–132 synaptic profiles from 4–12 mice.

Results

PKC involvement in slow and rapid endocytosis at calyces

We studied PKC-deficient mice because in preliminary studies, we noticed that a PKC inhibitor inhibited endocytosis at calyces. We generated $PKC_\alpha^{-/-}$ mice by breeding $PKC_\alpha^{+/-}$ mice from The Jackson Laboratory and generated $PKC_\beta^{-/-}$ mice by ourselves (Fig. 1*A*). Targeted embryonic stem cells ($Prkcb^{tm1a(EUCOMM)Wtsi}$ line EPD0233_5_F09) obtained from The International Mouse Phenotyping Consortium were injected into C57BL/6J blastocysts to generate chimeras (Fig. 1*A*). Chimeric mice were then bred with C57BL/6J mice to generate *PKC_β* targeted germline mice ($PKC_\beta^{+/loxP}$). $PKC_\beta^{+/loxP}$ mice were bred with CMV-Cre mice (The Jackson Laboratory, 006054) to delete exon 4 of PKC_β gene, which resulted in the generation of $PKC_\beta^{-/+}$ mice (Fig. 1*A*). $PKC_\beta^{-/+}$ mice were used to establish the $PKC_\beta^{-/-}$ mouse line (Fig. 1*A*).

In WT mice, immunostaining showed that PKC_α and PKC_β were colocalized with vesicular glutamate transporter 1 ($vGluT_1$) that labeled vesicles in P7–P10 calyces (Fig. 1*B*,*C*). These results revealed the presence of PKC_α and PKC_β at calyces. In $PKC_\alpha^{-/-}$ or $PKC_\beta^{-/-}$ mice, PKC_α or PKC_β was nearly absent at P7–P10 calyces, respectively (Fig. 1*B*–*D*). The remaining immunostaining was close to background staining (Fig. 1*B*–*D*). These results confirm successful deletion of PKC_α or PKC_β in $PKC_\alpha^{-/-}$ or $PKC_\beta^{-/-}$ mice calyces, respectively.

To determine whether PKC_α or PKC_β knock-out affects endocytosis, we performed whole-cell voltage-clamp recordings at P7–P10 mouse calyces at 22–24°C, if not mentioned otherwise. In WT calyces, a 20 ms depolarization from −80 mV to +10 mV ($depol_{20ms}$) induced a calcium current (I_{Ca}) of 1.65 ± 0.13 nA, and a capacitance (C_m) jump (ΔC_m) of 370 ± 43 fF ($n = 9$; Fig. 2*A*–*C*). After the jump, C_m decayed monoexponentially with a time constant (τ) of 18.5 ± 2.0 s, and an initial decay rate ($Rate_{decay}$) of 24 ± 3 fF/s ($n = 9$; Fig. 2*A*–*C*). We used $Rate_{decay}$ for statistics, because the decay time constant was often too slow to estimate within the recording time window when endocytosis is inhibited (Wu et al., 2009, 2016).

The $Rate_{decay}$ after $depol_{20ms}$ in $PKC_\alpha^{-/-}$ or $PKC_\beta^{-/-}$ calyces was reduced to ~32–46% of WT, whereas ΔC_m and I_{Ca} charge (QI_{Ca}) were not different (Fig. 2*A*–*C*). Similar reduction was observed in three conditions: 1) after 20 action potential-equivalent stimuli (APe, 1 ms from −80 to +7 mV) at 100 Hz (Fig. 2*D*,*E*), which also induced slow endocytosis in WT mice (Wu et al., 2009), 2) at 34–37°C (Fig. 2*F*), and 3) at P13–P14 calyces (Fig. 2*G*) that are more matured (Borst and Soria van Hoeve, 2012). These results suggest PKC_α and PKC_β involvement in slow endocytosis in various stimuli, temperatures and immature or mature synapses. Further supporting this suggestion, PKC inhibitor bisindolylmaleimide I (BIS, 5 μM, in the pipette solution) inhibited $Rate_{decay}$ after $depol_{20ms}$, whereas PKC enhancer phorbol-12-myristate-13-acetate (PMA, 1 μM, in the pipette solution) increased $Rate_{decay}$ at P7–P10 mouse calyces (Fig. 2*H*).

We applied 10 $depol_{20ms}$ at 10 Hz ($depol_{20msX10}$) to induce rapid endocytosis (Wu et al., 2009). In WT calyces, $depol_{20msX10}$ induced a ΔC_m of 1136 ± 126 fF, followed by a biexponential decay with τ of 1.9 ± 0.2 s (25 ± 3%) and 24.7 ± 1.6 s ($n = 9$; Fig. 3*A*,*B*), respectively. The $Rate_{decay}$ was 157 ± 22 fF/s ($n = 9$; Fig. 3*A*–*C*), which reflected mostly (~80%) the rapid component of endocytosis (Wu et al., 2009; Sun et al., 2010). The $Rate_{decay}$ in $PKC_\alpha^{-/-}$ and $PKC_\beta^{-/-}$ calyces decreased to ~22–25% of that in WT, whereas QI_{Ca} did not change significantly (Fig. 3*B*,*C*). Similar $Rate_{decay}$ reduction was observed in three conditions: (1) after 200 APe at 100 Hz (Fig. 3*D*,*E*), which also induced rapid endocytosis in WT (Wu et al., 2009), (2) at 34–37°C (Fig. 3*F*), and (3) in more matured P13–P14 calyces (Fig. 3*G*). These results suggest PKC_α and PKC_β involvement in rapid endocytosis. Further supporting this suggestion, PKC inhibitor BIS inhibited $Rate_{decay}$ after $depol_{20msX10}$ at P7–P10 mouse calyces (Fig. 3*H*). PKC enhancer PMA did not increase $Rate_{decay}$ (Fig. 3*H*), likely because $Rate_{decay}$ after $depol_{20msX10}$ was close to saturation (Wu et al., 2009).

$Rate_{decay}$ after $depol_{20ms}$ or $depol_{20msX10}$ at 34–37°C or P13–P14 calyces was larger than that at 22–24°C or P7–P10 calyces,

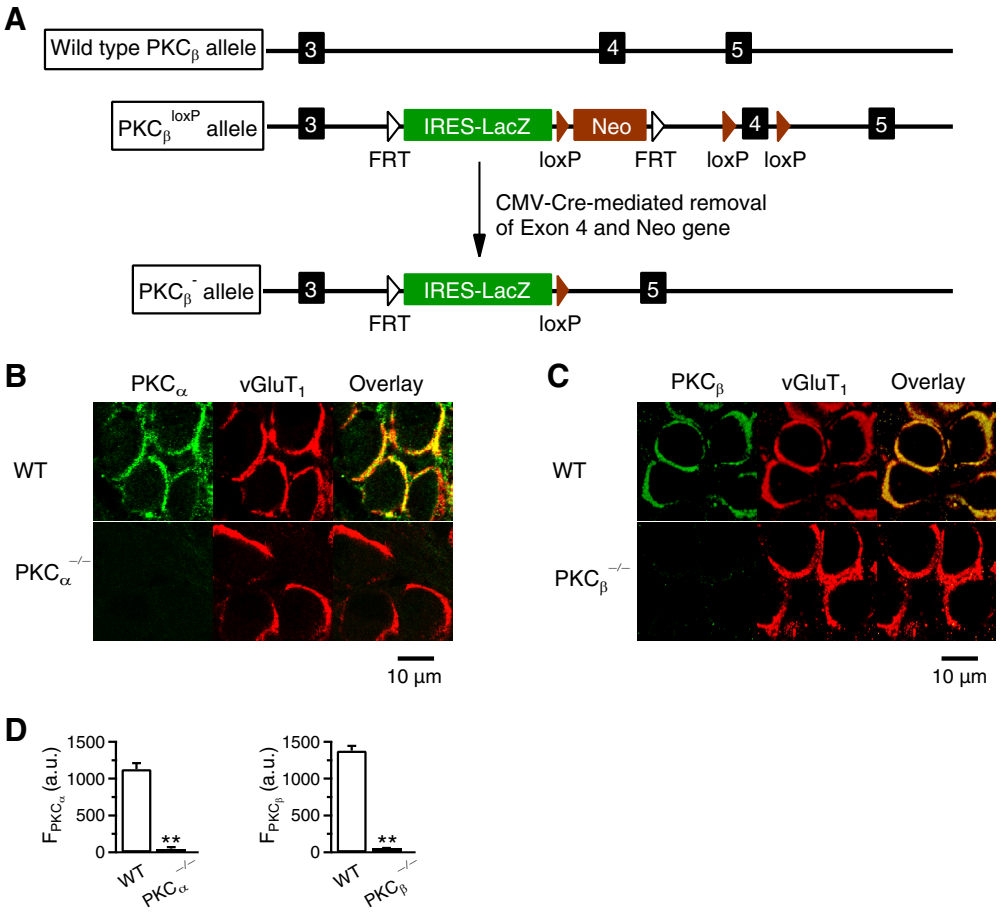

Figure 1. PKC knock-out mouse generation and immunostaining. ***A***, Schematic illustration of the generation of $PKC_{\beta}^{-/-}$ mice. PKC_{β} gene has five exons, three of which (3, 4, and 5) are shown. Targeted embryonic stem (ES) cells ($Prkcb^{tm1a(EUCOMM)Wtsi}$ line EPD0233_5_F09) were obtained from The International Mouse Phenotyping Consortium and were injected into C57BL/6J blastocysts to generate chimeras. Chimeric mice were then bred with C57BL/6J to generate PKC_{β} targeted germline mice ($PKC_{\beta}^{+/loxP}$). $PKC_{\beta}^{+/loxP}$ mice were bred with CMV-Cre mice (The Jackson Laboratory, 006054) to delete exon 4, generating $PKC_{\beta}^{-/+}$ mice, which were used to establish the $PKC_{\beta}^{-/-}$ mouse line. Mouse genotypes were determined by PCR. ***B***, Antibody staining of PKC_{α} and $vGluT_1$ in P9 WT and $PKC_{\alpha}^{-/-}$ calyces ("overlay"). ***C***, Antibody staining of PKC_{β} and $vGluT_1$ in P9 WT and $PKC_{\beta}^{-/-}$ calyces ("overlay"). ***D***, Left, PKC_{α} immunostaining staining intensity ($F_{PKC\alpha}$; a.u., arbitrary units; mean + SEM) in P7–P10 WT (14 calyces, 4 mice) and $PKC_{\alpha}^{-/-}$ calyces (15 calyces, 4 mice). $^{**}p < 0.01$ (*t* test). Right, PKC_{β} immunostaining staining intensity ($F_{PKC\beta}$) in P7–P10 WT (24 calyces, 3 mice) and $PKC_{\beta}^{-/-}$ calyces (16 calyces, 3 mice). $^{**}p < 0.01$ (*t* test).

respectively (Figs. 2*B*,*C*,*F*,*G*, 3*B*,*C*,*F*,*G*). These results are consistent with previous studies showing that endocytosis is faster at higher temperature and more mature calyces (Renden and von Gersdorff, 2007; Chanaday and Kavalali, 2018).

PKC involvement in vesicle mobilization to the readily releasable pool

In $PKC_{\alpha}^{-/-}$ and $PKC_{\beta}^{-/-}$ calyces, ΔC_m was reduced after $depol_{20msX10}$ or 200 APe at 100 Hz (Fig. 3*B–E*), but not after $depol_{20ms}$ or 20 APe at 100 Hz (Fig. 2*B–E*) that selectively depleted the readily releasable vesicle pool (RRP) (Wu et al., 2009). Consistently, the accumulated ΔC_m from the second to the 10^{th} $depol_{20ms}$ during $depol_{20msX10}$ in $PKC_{\alpha}^{-/-}$ and $PKC_{\beta}^{-/-}$ calyces was smaller than WT (Fig. 3*I*), suggesting that PKC facilitates RRP replenishment. This might reflect PKC in facilitating active zone clearance, because endocytosis may facilitate RRP replenishment via active zone clearance (Hosoi et al., 2009; Wu et al., 2009; L.G. Wu et al., 2014).

PKC calcium-binding domain is needed for endocytosis at hippocampal synapses

Western blot at $PKC_{\alpha}^{-/-}$ or $PKC_{\beta}^{-/-}$ hippocampal cultures showed that PKC_{α} or PKC_{β} were not expressed, whereas other endocytic proteins, including clathrin, dynamin and AP2 were not affected (Fig. 4*A*,*B*). In cultures transfected with pH-sensitive synaptophysin-pHluorin2X (SypH), a 10 s train of stimuli (1 ms/20 mA) at 40 Hz ($Train_{40Hz}$), which generated an action potential train, induced a SypH fluorescence (F_{SypH}) increase (ΔF) and then decrease (Fig. 4*C*), reflecting exocytosis and endocytosis, respectively. In WT at 22–24°C (applies if not mentioned otherwise), F_{SypH} decayed mono-exponentially with a τ of 20.0 ± 1.4 s, reflecting slow endocytosis; the initial decay rate ($Rate_{decay}$) was 4.6 ± 0.4%/s ($n = 14$ experiments, 7 cultures, each culture from 3–5 mice; Fig. 4*C*). In $PKC_{\alpha}^{-/-}$ cultures, F_{SypH} decay was slower with a $Rate_{decay}$ ~41% of WT (Fig. 4*C*).

Is the slower F_{SypH} decay due to slower reacidification or endocytosis? In $PKC_{\alpha}^{-/-}$ cultures, MES solution with a pH of 5.5 applied before $Train_{10s}$ quenched F_{SypH} to the background level and decreased F_{SypH} by ΔS (Fig. 4*D*), which reflected the preexisting SypH molecules at the plasma membrane. Washing out MES solution led to recovery of F_{SypH} to baseline (Fig. 4*D*). We then applied a 10 s train of stimuli and applied MES solution at 10 s after the stimulation train, at which F_{SypH} remained well above the baseline. F_{SypH} was quenched to a level similar to that in MES solution before the stimulation train (lower dotted line; Fig. 4*D*), but much lower than that predicted, if F_{SypH} decay is due to

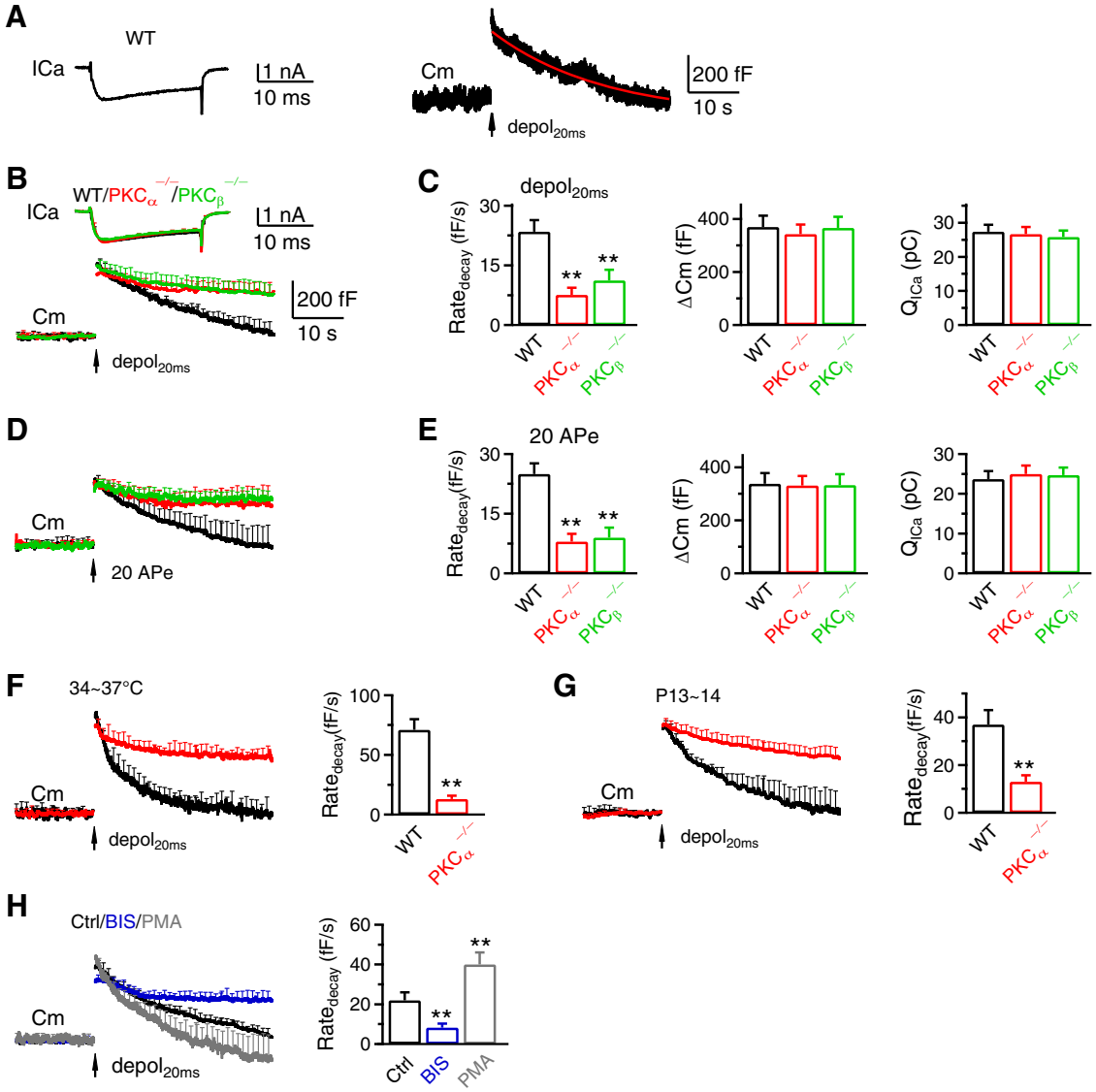

Figure 2. PKC_α or PKC_β knock-out inhibits slow endocytosis at calyces. ***A***, Sampled I_{Ca} (left) and C_m (right) induced by $depol_{20ms}$ (arrow) in a WT calyx. The red curve is a mono-exponential fit of the C_m decay with a τ of 19.1 s. (***B***) I_{Ca} (mean + SEM) and C_m (mean + SEM) induced by $depol_{20ms}$ (arrow) in WT (black, 9 calyces, 9 mice, abbreviated as 9c/9m), $PKC_\alpha^{-/-}$ (14c/14m, red) and $PKC_\beta^{-/-}$ (6c/6m, green) calyces. Data from P7–P10 mice at 22–24°C; SEM plotted every 2 ms for I_{Ca} and 1 s for C_m (applies to all similar graphs). ***C***, $Rate_{decay}$, the capacitance jump (ΔC_m) and the I_{Ca} charge (Q_{Ca}) induced by $depol_{20ms}$ in WT (9c/9m), $PKC_\alpha^{-/-}$ (14c/14m) and $PKC_\beta^{-/-}$ (6c/6m) calyces (P7–P10, 22–24°C). Bar graphs are plotted as mean + SEM (applies to all bar graphs) $^*p < 0.05$; $^{**}p < 0.01$; *t* test compared with WT (applies to all bar graphs). ***D***, ***E***, Similar to ***B*** and ***C***, respectively, except that the stimulus was 20 APe at 100 Hz (WT, 8c/8m; $PKC_\alpha^{-/-}$, 10c/10m; $PKC_\beta^{-/-}$, 8c/8m; P7–P10, 22–24°C). ***F***, ***G***, C_m and $Rate_{decay}$ (mean + SEM) induced by $depol_{20ms}$ (arrow) in WT (black, 7c/7m) and $PKC_\alpha^{-/-}$ calyces at 34–37°C (***F***; WT, 7c/7m; $PKC_\alpha^{-/-}$, 4c/4m; P7–P10 mice) or at P13–P14 mice (***G***: WT, 7c/7m; $PKC_\alpha^{-/-}$, 9c/9m; 22–24°C). (***H***) C_m and $Rate_{decay}$ (mean + SEM) induced by $depol_{20ms}$ in control (Ctrl, 11c/11m) or in the presence of BIS (11c/11m) or PMA (8c/8m) at 22–24°C in P7–P10 mice.

reacidification (upper dotted line; Fig. 4*D*, $n = 6$). Quenched F_{SypH} recovered above baseline after MES washout, confirming the prolonged presence of SypH at the plasma membrane (Fig. 4*D*). Thus, slower F_{SypH} decay in $PKC_\alpha^{-/-}$ cultures primarily reflected slower endocytosis.

Prolonged F_{SypH} decay and reduced $Rate_{decay}$ were also observed at 34–37°C (Fig. 4*E*, $PKC_\alpha^{-/-}$ culture), at $PKC_\beta^{-/-}$ culture (Fig. 4*F*), and after a 10 s action potential train at 20 Hz (Fig. 4*G*, $PKC_\alpha^{-/-}$ culture). $Rate_{decay}$ in $PKC_\alpha^{-/-}$ culture was rescued to the WT level by transfection of WT PKC_α, but not a mutant PKC_α (Fig. 4*H*), in which 5 aspartates in its calcium binding C2 domain were mutated to alanines ($PKC_\alpha^{D/A}$; Fig. 4*I*) (Nalefski and Falke, 1996).

$PKC_\alpha^{D/A}$ neither binds calcium nor is translocated to the plasma membrane by calcium as WT PKC (Newton, 2010) (D. Fiorovante and W. Regehr, personal communication. see also Fig. 4*J*). The fluorescence of mCherry was similar in $PKC_\alpha^{-/-}$ neurons overexpressed with PKC_α and mCherry or with $PKC_\alpha^{D/A}$ and mCherry (Fig. 4*K*, *t* test, $p = 0.84$), consistent with similar expression level of PKC_α and $PKC_\alpha^{D/A}$. Together, these results suggest that PKC calcium binding domain is needed for endocytosis. PKC may thus serve as an endocytosis calcium sensor.

EM suggests PKC involvement in endocytosis of regular vesicles and bulk endosomes

We performed EM to examine ultrastructural changes in $PKC_\alpha^{-/-}$ hippocampal cultures. Horseradish peroxidase (HRP, 5 mg/ml, bath) was added for assay of vesicular uptake. At rest, HRP-positive [HRP(+)] vesicles were minimal; most vesicles

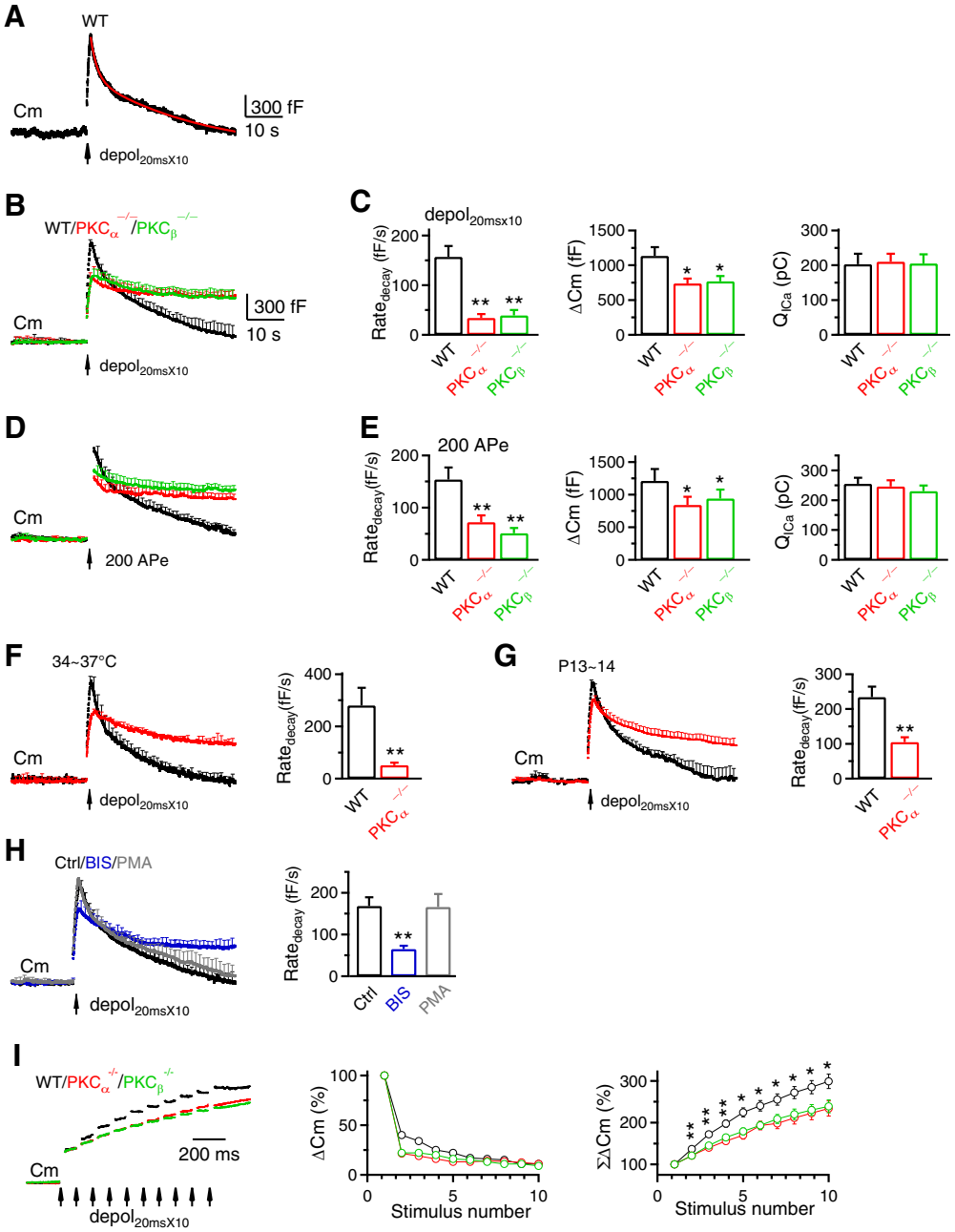

Figure 3. PKC_α or PKC_β knock-out inhibits rapid endocytosis and vesicle mobilization to the readily releasable pool at calyces. ***A–H***, Similar arrangements as Figure 2*A–H*, respectively, except that the stimulus was $depol_{20msX10}$ (***A–C***, ***F–H***) or 200 APe at 100 Hz (***D***,***E***) for inducing rapid endocytosis. ***A***, Red curve is a biexponential fit of the C_m decay with a τ of 1.4 s and 14.3 s, respectively (I_{Ca} not shown). ***B***, ***C***, WT, 9c/9m; $PKC_\alpha^{-/-}$, 14c/14m; $PKC_\beta^{-/-}$, 6c/6m. ***D***, ***E***, WT, 8c/8m; $PKC_\alpha^{-/-}$, 11c/11m; $PKC_\beta^{-/-}$, 8c/8m. ***F***, WT, 6c/6m; $PKC_\alpha^{-/-}$, 4c/4m. ***G***, WT, 7c/7m; $PKC_\alpha^{-/-}$, 8c/8m. ***H***, Ctrl, 11c/11m; BIS, 11c/11m; PMA, 8c/8m. ***I***, Left, Sampled C_m induced by $depol_{20msX10}$ (each arrow: 1 $depol_{20ms}$) from WT, $PKC_\alpha^{-/-}$ and $PKC_\beta^{-/-}$ calyces. ΔC_m induced by the first $depol_{20ms}$ was normalized. Middle and right, ΔC_m (middle) and accumulated ΔC_m ($\Sigma\Delta C_m$, right) induced by each of the 10 $depol_{20ms}$ during $depol_{20msX10}$ in WT (9c/9m), $PKC_\alpha^{-/-}$ (14c/14m) and $PKC_\beta^{-/-}$ (6c/6m) calyces. Data (mean ± SEM) are normalized to ΔC_m induced by the first $depol_{20ms}$. $\Sigma\Delta C_m$ was significantly higher for the WT group (*$p < 0.05$; **$p < 0.01$).

were HRP-negative [HRP(−)] (Fig. 5*A*,*B*); the number of HRP(+) and HRP(−) vesicles and their sum in boutons were similar in WT and $PKC_\alpha^{-/-}$ cultures (data not shown). To examine endocytosis, we applied 90 mM KCl with HRP for 1.5 min, and fixed samples at 0, 3 and 10 min after KCl/HRP application. In WT boutons, compared with the resting condition, HRP(+) vesicles increased from time 0 to 10 min after KCl, reflecting vesicle endocytosis (Fig. 5*A*,*B*) as previously shown (Y. Wu et al., 2014; Wu et al., 2016). Compared with WT boutons, HRP(+) vesicles were significantly reduced at each time point after KCl in $PKC_\alpha^{-/-}$ boutons (Fig. 5*A*,*B*), suggesting inhibition of endocytosis.

In WT boutons, we observed HRP(+) bulk endosomes (Fig. 5*A*), defined as vesicles with a diameter > 80 nm or with a cross section area more than that of a 80 nm vesicle (~0.005 μm^2). Bulk endosome area increased at time 0, then decreased at 3 and 10 min (Fig. 5*A*,*C*), suggesting generation of bulk endosomes and subsequent conversion to vesicles as previously shown (Y. Wu et al., 2014; Wu et al., 2016). Similar trends were observed in $PKC_\alpha^{-/-}$, but at a lower level, which was significant at 10 min time point (Fig. 5*C*), suggesting inhibition of bulk endocytosis. These EM data confirmed the involvement of PKC in endocytosis. Results shown in Figure 5, *A–C*, were obtained at room temperature (22–24°C). Results similar to

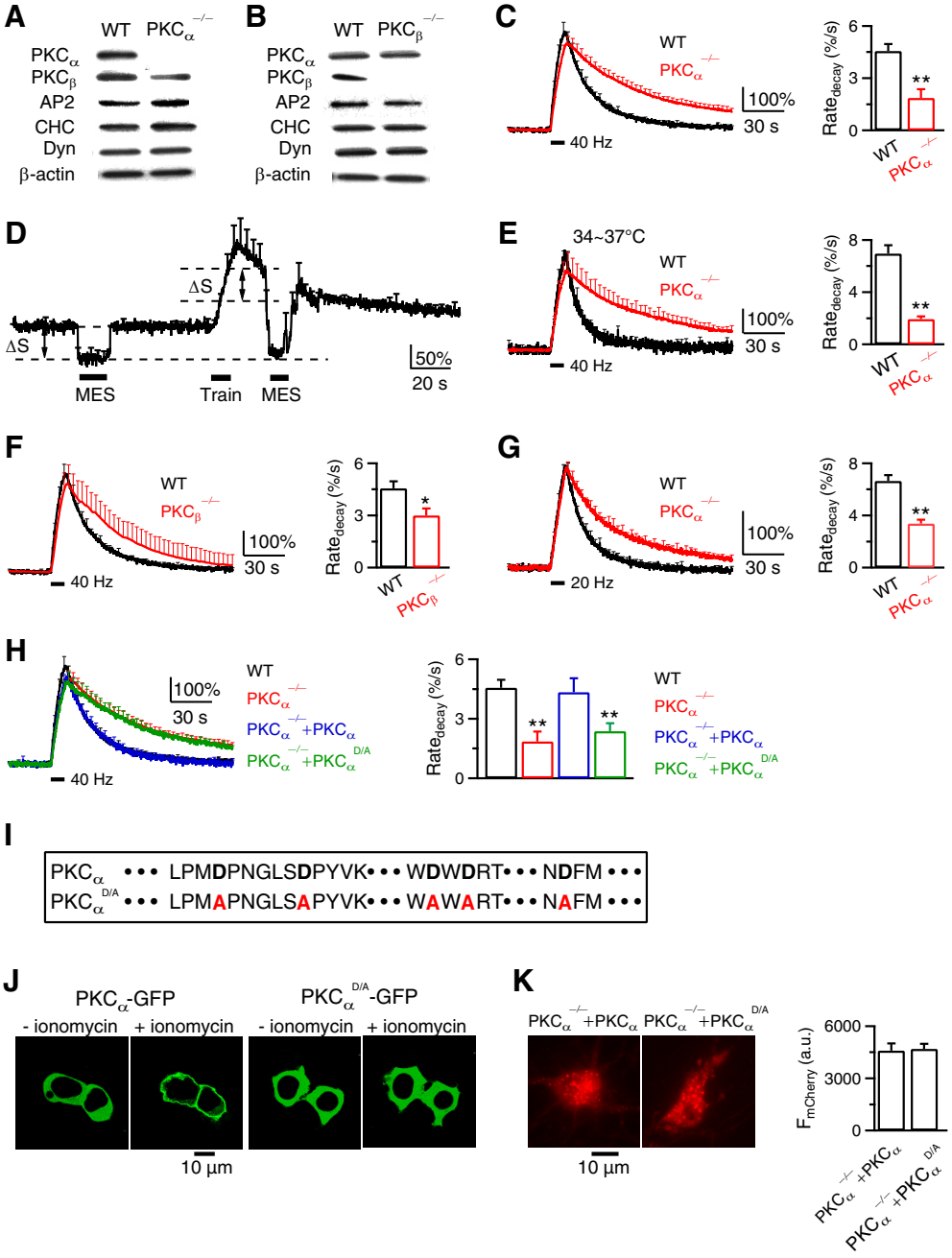

Figure 4. PKC and its calcium-binding domain are required for endocytosis at hippocampal synapses. ***A***, ***B***, Western blot of PKC_{α}, PKC_{β}, adaptor protein 2 (AP2), clathrin heavy chain (CHC), dynamin (Dyn), and β-actin in WT, $PKC_{\alpha}^{-/-}$ (***A***), and $PKC_{\beta}^{-/-}$ (***B***) hippocampal culture. Results in ***A*** and ***B*** were repeated by 2–4 times. ***C***, F_{SypH} traces (normalized to baseline, left) and $Rate_{decay}$ (right) induced by $Train_{40Hz}$ (bar) in WT ($n = 14$ experiments) or $PKC_{\alpha}^{-/-}$ ($n = 28$ experiments) hippocampal culture at 22–24°C. Data plotted as mean + SEM; $^{*}p < 0.05$; $^{**}p < 0.01$, *t* test (applies to all similar graphs). Throughout the study, each experiment contained 20–30 boutons; 1–3 experiments were taken from 1 culture; each culture was from 3–5 mice; each group was from 4–12 cultures. ***D***, Applying MES solution (pH:5.5, bars) quenched F_{SypH} (mean + SEM) to a similar level (lowest dash line) before and after a 10 s train of stimuli in $PKC_{\alpha}^{-/-}$ boutons ($n = 6$ experiments, 22–24°C). ΔS, SypH at resting plasma membrane quenched by MES. ***E–G***, Similar to ***C***, but at 34–37°C (***E***), in $PKC_{\beta}^{-/-}$ culture (***F***), or after a 10 s train at 20 Hz (***G***). ***E***, WT, $n = 6$ experiments; $PKC_{\alpha}^{-/-}$, $n = 6$. ***F***, WT, $n = 14$; $PKC_{\beta}^{-/-}$, $n = 5$. ***G***, WT, $n = 16$; $PKC_{\alpha}^{-/-}$, $n = 22$. ***H***, F_{SypH} traces and $Rate_{decay}$ induced by $Train_{40Hz}$ (bar) in WT boutons ($n = 14$), $PKC_{\alpha}^{-/-}$ boutons ($PKC_{\alpha}^{-/-}$, $n = 28$), $PKC_{\alpha}^{-/-}$ boutons rescued with WT PKC_{α} (containing mCherry for recognition, $PKC_{\alpha}^{-/-} + PKC_{\alpha}$, $n = 7$), and in $PKC_{\alpha}^{-/-}$ boutons rescued with $PKC_{\alpha}^{D/A}$ and mCherry ($PKC_{\alpha}^{-/-} + PKC_{\alpha}^{D/A}$, $n = 8$). ***I***, Protein sequence of PKC_{α} and $PKC_{\alpha}^{D/A}$ C2 domain. The Ca^{2+}-coordinating aspartates of PKC_{α} (bold) were mutated to alanines (red) in $PKC_{\alpha}^{D/A}$. ***J***, We expressed $PKC_{\alpha\text{-GFP}}$ (left two panels) or $PKC_{\alpha}^{D/A}$-GFP (right two panels) in HEK293T cells and monitored the subcellular distribution of the kinase. The Ca^{2+} ionophore, ionomycin (10 μM, 15 min), induced translocation of $PKC_{\alpha\text{-GFP}}$ toward the plasma membrane, but did not alter the intracellular distribution of $PKC_{\alpha}^{D/A}$-GFP. Such results were observed in 3 experiments (each experiment had 2–3 cells). ***K***, Left, $PKC_{\alpha}^{-/-}$ neurons rescued with WT PKC_{α} (containing mCherry for recognition, $PKC_{\alpha}^{-/-} + PKC_{\alpha}$), or with $PKC_{\alpha}^{D/A}$ and mCherry ($PKC_{\alpha}^{-/-} + PKC_{\alpha}^{D/A}$). Right, Fluorescence intensity of mCherry ($F_{mCherry}$) in $PKC_{\alpha}^{-/-} + PKC_{\alpha}$ neurons ($n = 10$) and $PKC_{\alpha}^{-/-} + PKC_{\alpha}^{D/A}$ neurons ($n = 13$). $F_{mCherry}$ was measured from both soma and branches.

Figure 5, *A–C*, were also observed at physiological temperature (37°C; Fig. 5*D*,*E*), at which bulk endocytosis was more severely inhibited, suggesting more involvement of PKC in bulk endocytosis in physiological temperature.

While we examined bulk endocytosis with EM at a time scale of minutes, this does not mean that bulk endocytosis is completely independent of rapid and slow endocytosis measured at live synapses. Bulk endocytosis detected with capacitance measurements

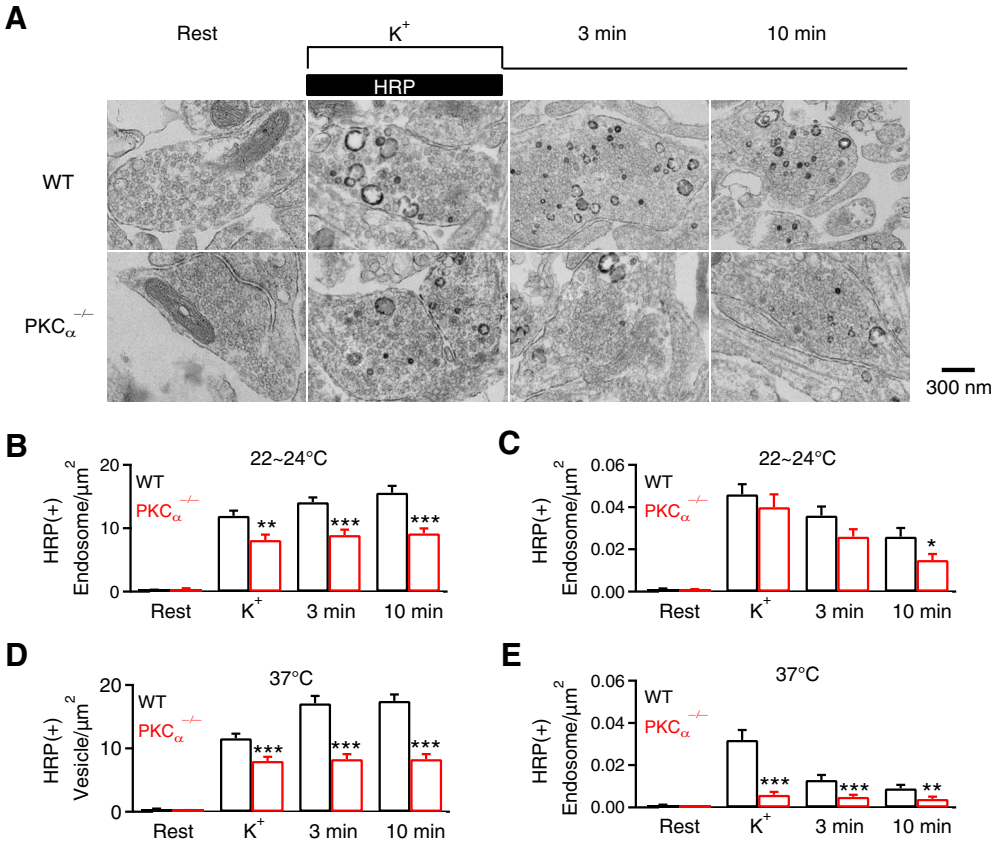

Figure 5. PKC_{α} knock-out affects endocytosis examined with EM at hippocampal synapses. ***A***, EM images of WT and $PKC_{\alpha}^{-/-}$ hippocampal boutons at rest (Rest) and at 0 min (K^+), 3 min and 10 min after 1.5 min 90 mM KCl application. For Rest, HRP was included for 1.5 min; for KCl application, HRP was included only during KCl application (see labels). ***B***, ***C***, Number of HRP(+) vesicles (***B***) and the bulk endosome area (***C***) per square micrometer of synaptic cross-section are plotted versus the time before (Rest) and at 0 min (K^+), 3 min, and 10 min after the end of KCl application in WT and $PKC_{\alpha}^{-/-}$ hippocampal cultures (mean + SEM, each group was from 100–132 synaptic profiles from 4–12 mice). The temperature before fixation was 22–24°C. ***$p < 0.001$; **$p < 0.01$; *$p < 0.05$ (*t* test). ***D***, ***E***, Similar to ***B*** and ***C***, respectively, except that the temperature was 37°C before fixation.

can be rapid or slow, within ~1–20 s after stimuli, and contributed to mediating rapid and slow endocytosis (Wu and Wu, 2007). Bulk endocytosis detected with EM after rapid freezing can be ultrafast, within hundreds of milliseconds after an action potential like stimulation in physiological temperature (Watanabe et al., 2013). Thus, rapid and slow endocytosis may be due to formation of bulk endosome-like structures as well as regular-size vesicles.

Calmodulin involvement in slow and rapid endocytosis at calyces

Pharmacology and knock-down experiments suggest CaM involvement in endocytosis (Wu et al., 2009; Sun et al., 2010; Yamashita et al., 2010; Yao and Sakaba, 2012). Here we verified this suggestion by gene knock-out, and more importantly, determined whether calcium binding with CaM is needed, the basic criteria for being a calcium sensor. Among 3 CaM genes (*CaM1*, *CaM2*, and *CaM3*) encoding the same CaM, we generated CaM_2^{loxP} mice by CRISPR technique as illustrated in Figure 6*A*. sgRNAs were designed by using CRISPR Design (https://zlab.bio/guide-design-resources) to identify unique target sites throughout the mouse genome (Fig. 6*A*). sgRNAs were transcribed *in vitro* using the MEGAshortscript T7 Transcription Kit from synthetic double-strand DNAs and purified using MEGAclear kit (Fig. 6*A*). A mixture of Cas9 mRNA, sgRNAs and ssDNA templates was injected into the cytoplasm of one cell-stage fertilized embryos harvested from C57BL/6J mice (Fig. 6*A*). Viable two-cell stage embryos were transferred into the oviducts of female surrogates to generate founder mice (Fig. 6*A*). Founders with loxP inserts were identified by PCR and sequencing, and were subsequently bred with C57BL/6J mice to generate heterozygous mice (Fig. 6*A*). CaM_2^{loxP} mouse was crossed with CMV-Cre mouse to generate $CaM_2^{-/-}$ mouse.

In $CaM_2^{-/-}$ calyces, immunostaining showed significant reduction of CaM (Fig. 6*B*); $Rate_{decay}$ after $depol_{20ms}$ and $depol_{20msX10}$ was significantly reduced at 22–24°C at P7–P10 calyces (Fig. 6*C*,*D*). Similar reduction of $Rate_{decay}$ was observed at 34–37°C (Fig. 6*E*, *F*; P7–P10 calyces) or P13–P14 calyces (Fig. 6*G*,*H*, 22–24°C). These results suggest CaM involvement in slow and rapid endocytosis, consistent with previous pharmacology studies at calyces (Wu et al., 2009; Yao and Sakaba, 2012).

CaM involvement in vesicle mobilization to the readily releasable pool

The ΔC_m after $depol_{20msX10}$ was reduced (Fig. 6*D*,*F*,*H*). This result provided the genetic evidence supporting the previous suggestion that CaM mediates calcium-dependent RRP replenishment, likely via active zone clearance (Hosoi et al., 2009; Wu et al., 2009; L.G. Wu et al., 2014).

Calmodulin calcium binding domain is needed for endocytosis at hippocampal synapses

In $CaM_2^{-/-}$ hippocampal synapses, Western blot showed significant reduction of CaM, but not other major endocytic proteins (Fig. 7*A*,*B*); $Rate_{decay}$ was significantly reduced after a 40 or 20 Hz train, particularly the 40 Hz train at either 22–24°C or 34–37°C

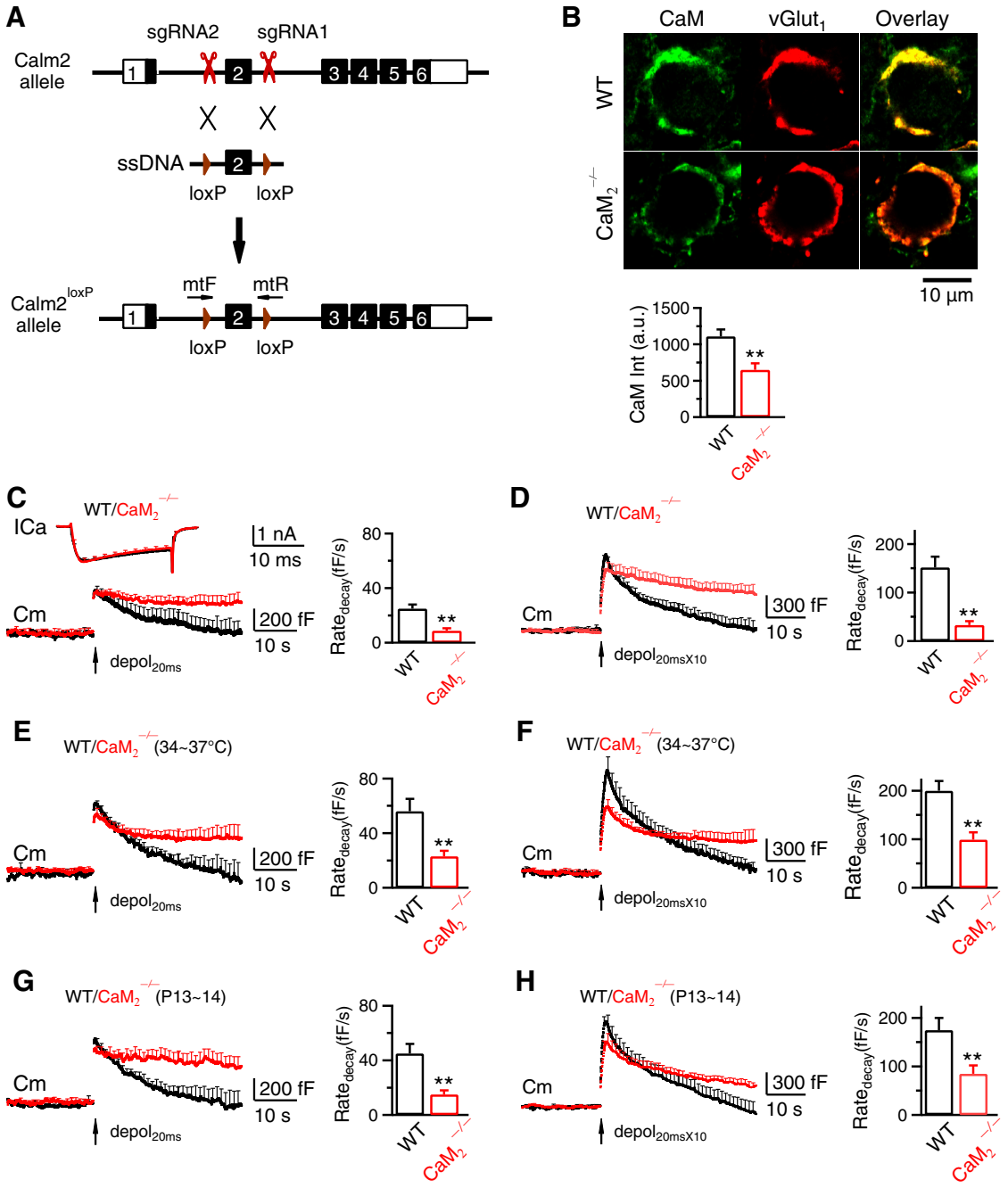

Figure 6. CaM 2 knock-out inhibits slow endocytosis, rapid endocytosis, and vesicle mobilization to the readily releasable pool at calyces. ***A***, Generation of *Calm2*^{loxP} mice (*Calm2:* Calmodulin 2 gene). sgRNAs were designed by using CRISPR Design (https://zlab.bio/guide-design-resources) to identify unique target sites throughout the mouse genome. sgRNAs were transcribed *in vitro* using the MEGAshortscript T7 Transcription Kit (Life Technologies) from synthetic double-strand DNAs purchased from IDT (Integrated DNA Technologies) and purified using MEGAclear kit (Life Technologies). A mixture of Cas9 mRNA (TriLink Biotechnologies, 100 ng/μl), sgRNAs (50 ng/μl), and ssDNA templates (100 ng/μl, synthesized by IDT) was injected into the cytoplasm of one cell-stage fertilized embryos harvested from C57BL/6J mice (The Jackson Laboratory, 000664). Viable two-cell stage embryos were transferred into the oviducts of female surrogates to generate founder mice. Founders with loxP inserts were identified by PCR and sequencing, and were subsequently bred with C57BL/6J mice to generate heterozygous mice. The primers used to identify the 5′ and 3′ loxP insertions were Calm2 mtF: 5′-CCATGAACCTTGAACCTGTAGGATCCA-3′ and Calm2 mtR: 5′-ATGCTACATTCAACTTGTCACCATTCGAATTCA-3′. ***B***, Top, Antibody staining of CaM and vGluT$_1$ (labeling calyx) in a P9 WT (upper) and a CaM$_2$ $^{-/-}$ (lower) calyx (images superimposed in the right). Bottom, CaM staining intensity (mean + SEM, a.u., arbitrary unit) in P7–P10 WT (47 calyces, 4 mice) and CaM$_2$ $^{-/-}$ calyces (53 calyces, 4 mice). $^{**}p < 0.01$ (*t* test). ***C***, I_{Ca}, C_m and Rate$_{decay}$ (mean + SEM) induced by depol$_{20ms}$ (arrow) in WT (8c/8m, black) and CaM$_2$ $^{-/-}$ (9c/9m) calyces (P7–P10, 22–24°C). ***D***, Similar to ***C***, but with depol$_{20msX10}$ (WT, 8c/8m; CaM$_2$ $^{-/-}$, 9c/9m). ***E***, ***F***, Similar to ***C*** and ***D***, respectively, but at 34–37°C. ***E***, WT, 6c/6m; CaM$_2$ $^{-/-}$, 6c/6m. ***F***, WT, 6c/6m; CaM$_2$ $^{-/-}$, 6c/6m. ***G***, ***H***, Similar to ***C*** and ***D***, respectively, but from P13–P14 calyces. ***G***, WT, 7c/7m; CaM$_2$ $^{-/-}$, 8c/8m. ***H***, WT, 7c/7m; CaM$_2$ $^{-/-}$, 8c/8m.

(Fig. 7*C–E*). Consistently, the time course of F_{SypH} decay at CaM$_2$ $^{-/-}$ synapses was slower (Fig. 7*C–E*). The slower F_{SypH} decay was not due to slower reacidification, as revealed with acid-quenching of surface SypH (data not shown). Thus, CaM$_2$ knock-out inhibits endocytosis, consistent with previous knock-down experiments (Sun et al., 2010).

The Rate$_{decay}$ was rescued to the WT level by transfecting CaM$_2$ $^{-/-}$ culture with SypH and WT CaM cDNA, but not with

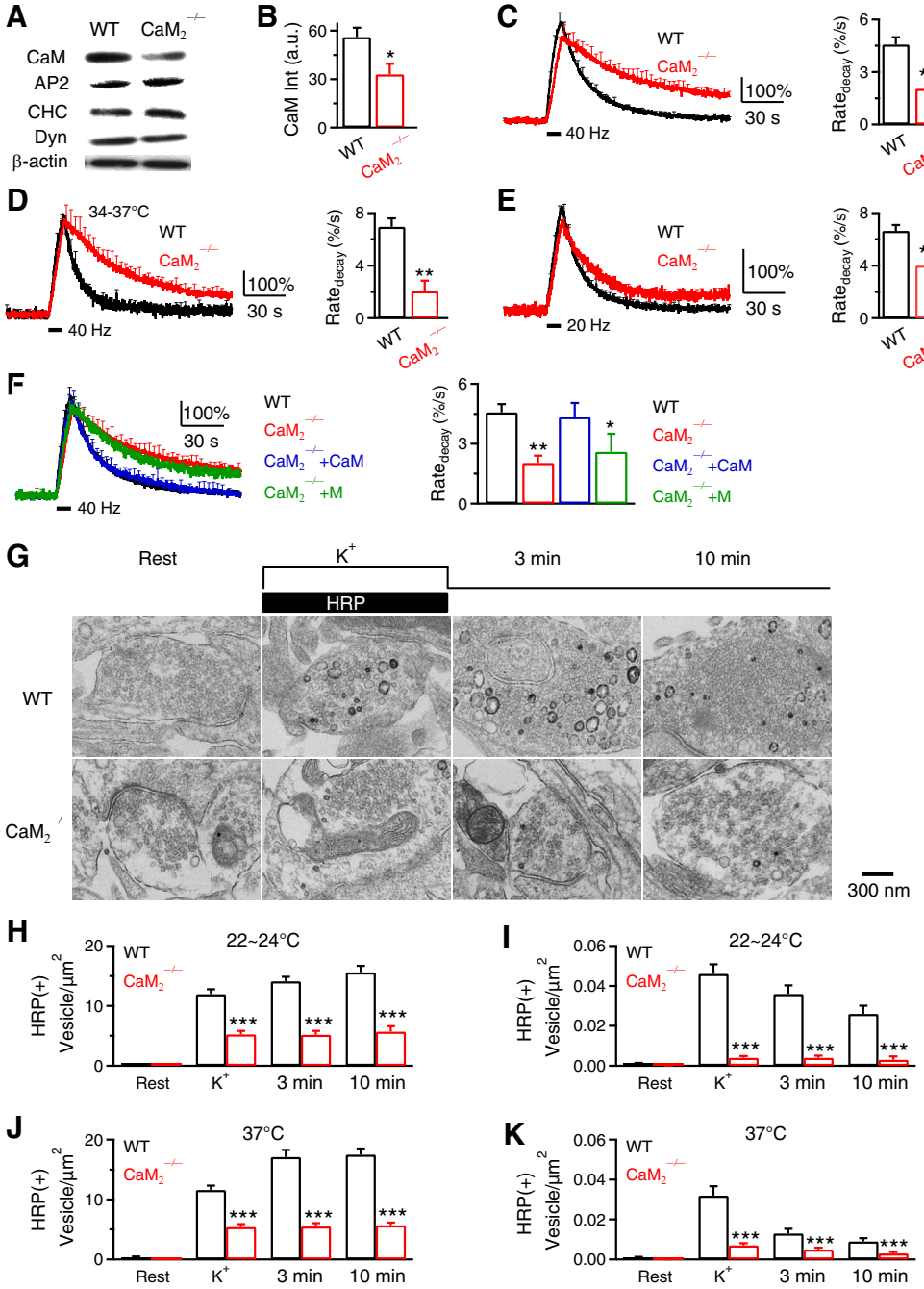

Figure 7. Calmodulin and its calcium binding domain are required for endocytosis at hippocampal synapses. ***A***, Western blot of CaM, AP2, clathrin heavy chain (CHC), dynamin (Dyn), and β-actin in WT and $CaM_2^{-/-}$ brain. ***B***, CaM Western blot intensity (CaM Int, a.u.) from WT or $CaM_2^{-/-}$ culture. ***C***, F_{SypH} traces (normalized to baseline) and $Rate_{decay}$ induced by $Train_{40Hz}$ (bar) in WT ($n = 14$ experiments) or $CaM_2^{-/-}$ ($n = 8$) hippocampal culture at 22–24°C (mean + SEM). ***D***, Similar to ***C***, but at 34–37°C (WT, $n = 6$; $CaM_2^{-/-}$, $n = 4$). ***E***, Similar to ***C***, but after a 10 s train at 20 Hz (WT, $n = 16$; $CaM_2^{-/-}$, $n = 7$). ***F***, F_{SypH} traces and $Rate_{decay}$ induced by $Train_{40Hz}$ in WT hippocampal boutons ($n = 14$ experiments, with SypH transfection), $CaM_2^{-/-}$ boutons ($n = 8$, with SypH transfection), $CaM_2^{-/-}$ boutons transfected with a plasmid containing CaM and mCherry (mCherry for recognition, SypH was cotransfected, $n = 4$, $CaM_2^{-/-}$+CaM), and $CaM_2^{-/-}$ boutons transfected with a plasmid containing CaM_{1234} and mCherry ($n = 4$, $CaM_2^{-/-}$+M). Temperature was 22–24°C. ***G***, EM images of WT and $CaM_2^{-/-}$ hippocampal boutons at rest (Rest) and at 0 min (K^+), 3 min and 10 min after 1.5 min application of KCl and HRP (same arrangements as in Fig. 5*A*). ***H***, ***I***, The number of HRP(+) vesicles (***H***) and the bulk endosome area (***I***) per square micrometer of synaptic cross-section are plotted versus the time before (Rest) and at 0 min (K^+), 3 min, and 10 min after KCl/HRP application in WT and $CaM_2^{-/-}$ hippocampal cultures (22–24°C). Data are expressed as mean + SEM; each group was from 100–132 synaptic profiles from 4–12 mice. ***J***, ***K***, Similar to ***H*** and ***I***, respectively, except that the temperature was 37°C.

SypH and CaM_{1234} mutant cDNA (Fig. 7*F*) where mutation in four calcium binding sites prevents calcium binding with CaM_{1234} (Xia et al., 1998). Thus, the calcium binding domain of CaM is needed to rescue endocytosis, suggesting that CaM serves as a calcium sensor.

EM suggests CaM involvement in endocytosis of regular vesicles and bulk endosome

We examined $CaM_2^{-/-}$ hippocampal cultures with the same EM approach used for PKC knock-out. HRP(+) vesicles were minimal at rest, but increased at 0–10 min after KCl application in

WT, which reflected vesicle endocytosis (Fig. 7*G*,*H*). The increase of the HRP(+) vesicle number was substantially inhibited in $CaM_2^{-/-}$ boutons (Fig. 7*G*,*H*), confirming inhibition of endocytosis in $CaM_2^{-/-}$ boutons. HRP(+) bulk endosome was significantly reduced to near 0 at each time point (0–10 min) after KCl application in $CaM_2^{-/-}$ boutons (Fig. 7*I*), suggesting involvement of CaM in bulk endocytosis. While results in Figure 7, *G–I*, were observed at room temperature, similar results were observed at physiological temperature (37°C; Fig. 7*J*,*K*), suggesting calmodulin involvement in endocytosis at both room and physiological temperature.

Discussion

We showed that PKC_α and PKC_β knock-out, generated by The Jackson Laboratory and by us (Fig. 1), inhibited slow and rapid endocytosis after various stimulation protocols in P7–P14 calyces at 22–37°C (Figs. 2, 3). PKC_α and PKC_β knock-out inhibited slow endocytosis measured with SypH imaging after action potential trains at 20–40 Hz at cultured hippocampal synapses at 22–37°C. This inhibitory effect (by PKC_α knock-out) was rescued by overexpressing WT PKC_α, but not $PKC_\alpha^{D/A}$ that could not bind calcium (Fig. 4). We generated $CaM_2^{-/-}$ mice and found that CaM_2 knock-out inhibited slow and rapid endocytosis at calyces (Fig. 6), and inhibited slow endocytosis at hippocampal synapses, which could be rescued by overexpressing WT CaM, but not CaM_{1234} that could not bind calcium (Figs. 6, 7). EM showed that PKC_α and CaM_2 knock-out reduced HRP(+) vesicles and HRP(+) bulk endosomes generated via bulk endocytosis (Figs. 5, 7). Together, these results suggest that calcium binding with the calcium sensor PKC_α, PKC_β and CaM mediate calcium-dependent trigger and speed up of slow, rapid and bulk endocytosis at synapses.

Early studies showed that PKC phosphorylates dynamin 1 and prevents dynamin 1 interaction with membrane phospholipids *in vitro* (Robinson et al., 1993; Powell et al., 2000). However, a subsequent study from the same lab shows that cyclin-dependent kinase 5, but not PKC phosphorylates dynamin 1 *in vivo* (Tan et al., 2003). The role of PKC in endocytosis has since not been considered. The present work suggests that calcium binding with PKC mediates calcium-stimulated slow and rapid endocytosis. PKC might stimulate endocytosis via phosphorylating serine/threonine of its substrates (Cousin and Robinson, 2001).

Studies with pharmacology and knock-down suggest CaM involvement in endocytosis (Wu et al., 2009; Sun et al., 2010; Yamashita et al., 2010; Yao and Sakaba, 2012). By knocking out *CaM_2* gene, we provided the first genetic evidence suggesting CaM involvement in rapid and bulk endocytosis (Figs. 6, 7), and the first knock-out evidence suggesting CaM involvement in slow endocytosis. Furthermore, by performing rescue experiments, we provided the missing evidence showing that CaM serves as a calcium sensor for endocytosis (Fig. 7). Potential downstream targets of CaM may include CaN and/or myosin light chain kinase (MLCK) for three reasons. First, both CaN and MLCK are activated by CaM; second, CaN dephosphorylates many endocytic proteins, and CaN knock-out inhibits endocytosis at calyceal, hippocampal and cerebellar synapses; and third, MLCK, which is involved in controlling the readily releasable pool size (Srinivasan et al., 2008), facilitates endocytosis via actomyosin interaction, and actin is essential for synaptic vesicle endocytosis (Cousin and Robinson, 2001; Sun et al., 2010; X.S. Wu et al., 2014; Yue and Xu, 2014; Delvendahl et al., 2016; Li et al., 2016; Wu et al., 2016; Soykan et al., 2017).

Calcium influx triggers endocytosis within a microdomain (hundreds of nanometers) at immature P7–P9 calyces, but within a nanodomain (tens of nanometers) at more mature P13–P14 or older calyces (Yamashita et al., 2010). Pharmacological blockers of CaM and calcineurin inhibited endocytosis at P7–P9 calyces, but not at P13–P14 calyces (Yamashita et al., 2010), leading to the proposal that endocytosis is independent of CaM and calcineurin at more matured calyces. However, calcineurin (X.S. Wu et al., 2014) and CaM_2 (Fig. 6) gene knock-out inhibit endocytosis at both P7–P10 and P13–P14 calyces. In contrast, calcineurin and calmodulin blockers slowed down endocytosis at a relatively small calcium influx, but did not inhibit endocytosis at a large calcium influx (X.S. Wu et al., 2014). These results might explain the difficulty of CaM and calcineurin blockers in inhibiting endocytosis at P13–P14 calyces, where much higher calcium concentration at the nanodomain of the calcium influx triggers endocytosis (Yamashita et al., 2010).

We do not know why endocytosis involves two calcium sensors, PKC and CaM. Given that PKC mediates phosphorylation, and CaM may activate CaN or MLCK to mediate dephosphorylation or phosphorylation (Cousin and Robinson, 2001; Yue and Xu, 2014), we suggest that calcium triggers and facilitates endocytosis by phosphorylation and dephosphorylation of the endocytosis machinery. Since endocytosis may be composed of multiple steps, such as formation of a membrane pit, formation of a narrow pore, hemi-fission, and fission (Kononenko and Haucke, 2015; Zhao et al., 2016; Mettlen et al., 2018; Shin et al., 2018), it might be possible that PKC and CaM are involved in these different transitions.

Knock-out or knock-down of synaptotagmin 1 led to slowdown of endocytosis, raising the possibility that synaptotagmin 1 may be another calcium sensor for endocytosis (Nicholson-Tomishima and Ryan, 2004; Poskanzer et al., 2006; Yao et al., 2011; Yao et al., 2012). However, a recent study shows that slower endocytosis in synaptotagmin 1 knock-out synapses is due to asynchronous vesicle fusion caused by synaptotagmin 1 knock-out (Li et al., 2017). Endocytosis after asynchronous fusion is slower than that after synchronous fusion, suggesting that synaptotagmin 1 is not an endocytosis calcium sensor (Li et al., 2017).

While the evidence for transient calcium influx in stimulating endocytosis is overwhelming in a variety of stimulation conditions (see introduction), it has been suggested that prolonged calcium dialysis or calcium after a single action potential may not facilitate endocytosis, but inhibit endocytosis (von Gersdorff and Matthews, 1994; Leitz and Kavalali, 2011; Wu and Wu, 2014; Li et al., 2017). Caution is therefore needed when considering our findings in these conditions. It should be noted that a 1 ms APe induces rapid endocytosis with a τ of ~2 s, whereas $depol_{20ms}$ induces slow endocytosis with a τ of ~15–20 at calyces (Wu et al., 2005). Similar results were observed at goldfish bipolar synapses and cerebellar mossy fiber boutons (von Gersdorff and Matthews, 1994; Delvendahl et al., 2016). These observations may be explained by the prolonged global calcium increase caused by increased depolarization, which has been shown to inhibit endocytosis (von Gersdorff and Matthews, 1994; Wu and Wu, 2014). Saturation of the endocytosis capacity, as previously proposed (Sankaranarayanan and Ryan, 2000; Sun et al., 2002; Wu et al., 2005) might also contribute to this observation.

Calcium triggers many forms of endocytosis, including rapid, slow, bulk, and overshoot endocytosis in nerve terminals (L.G. Wu et al., 2014), endocrine cells (Artalejo et al., 1995; Chiang et al., 2014; L.G. Wu et al., 2014) and dendrites (Kennedy and Ehlers, 2006). Our finding that calcium binding with the calcium

sensor PKC and CaM mediates calcium-stimulated endocytosis may apply to these calcium-dependent forms of endocytosis in neurons and endocrine cells. It might also apply to the calcium-triggered fusion pore (Chiang et al., 2014; Shin et al., 2018) and fission pore closure (Wu et al., 2009) that control exo- and endocytosis efficiency, and to calcium- and endocytosis-dependent RRP replenishment that sustains synaptic transmission.

Endocytosis has been suggested to help sustain synaptic transmission during repetitive activity by facilitating the RRP replenishment via clearance of the fusing vesicle membrane and proteins at the active zone (Hosoi et al., 2009; Wu et al., 2009; Neher, 2010; Hua et al., 2013; L.G. Wu et al., 2014). CaM_2 knock-out slowed down the RRP replenishment at calyces (Fig. 6), which provides the missing genetic evidence supporting previous pharmacological studies that suggest CaM involvement in calcium-dependent vesicle mobilization to the RRP (Sakaba and Neher, 2001; Wu et al., 2009). PKC_α and PKC_β knock-out also slowed down the RRP replenishment at calyces (Fig. 3), suggesting that PKC is also involved in calcium-dependent RRP replenishment. Calcium binding with PKC and CaM may thus mediate calcium-facilitated (and endocytosis-dependent) replenishment of releasable vesicles to sustain exocytosis in nerve terminals and non-neuronal secretory cells.

References

Artalejo CR, Henley JR, McNiven MA, Palfrey HC (1995) Rapic endocytosis coupled to exocytosis in adrenal chromaffin cells involves Ca^{2+}, GTP, and dynamin but not clathrin. Proc Natl Acad Sci U S A 92:8328–8332.

Balaji J, Armbruster M, Ryan TA (2008) Calcium control of endocytic capacity at a CNS synapse. J Neurosci 28:6742–6749.

Borst JG, Soria van Hoeve J (2012) The calyx of Held synapse: from model synapse to auditory relay. Annu Rev Physiol 74:199–224.

Chanaday NL, Kavalali ET (2018) Time course and temperature dependence of synaptic vesicle endocytosis. FEBS Lett 592:3606–3614.

Chiang HC, Shin W, Zhao WD, Hamid E, Sheng J, Baydyuk M, Wen PJ, Jin A, Momboisse F, Wu LG (2014) Post-fusion structural changes and their roles in exocytosis and endocytosis of dense-core vesicles. Nat Commun 5:3356.

Clayton EL, Anggono V, Smillie KJ, Chau N, Robinson PJ, Cousin MA (2009) The phospho-dependent dynamin-syndapin interaction triggers activity-dependent bulk endocytosis of synaptic vesicles. J Neurosci 29:7706–7717.

Cottrell JR, Li B, Kyung JW, Ashford CJ, Mann JJ, Horvath TL, Ryan TA, Kim SH, Gerber DJ (2016) Calcineurin agamma is a functional phosphatase that modulates synaptic vesicle endocytosis. J Biol Chem 291:1948–1956.

Cousin MA, Robinson PJ (2001) The dephosphins: dephosphorylation by calcineurin triggers synaptic vesicle endocytosis. Trends Neurosci 24:659–665.

Delvendahl I, Vyleta NP, von Gersdorff H, Hallermann S (2016) Fast, temperature-sensitive and clathrin-independent endocytosis at central synapses. Neuron 90:492–498.

Hosoi N, Holt M, Sakaba T (2009) Calcium dependence of exo- and endocytotic coupling at a glutamatergic synapse. Neuron 63:216–229.

Hua Y, Woehler A, Kahms M, Haucke V, Neher E, Klingauf J (2013) Blocking endocytosis enhances short-term synaptic depression under conditions of normal availability of vesicles. Neuron 80:343–349.

Kennedy MJ, Ehlers MD (2006) Organelles and trafficking machinery for postsynaptic plasticity. Annu Rev Neurosci 29:325–362.

Kononenko NL, Haucke V (2015) Molecular mechanisms of presynaptic membrane retrieval and synaptic vesicle reformation. Neuron 85:484–496.

Leitz J, Kavalali ET (2011) Ca(2)(+) influx slows single synaptic vesicle endocytosis. J Neurosci 31:16318–16326.

Li L, Wu X, Yue HY, Zhu YC, Xu J (2016) Myosin light chain kinase facilitates endocytosis of synaptic vesicles at hippocampal boutons. J Neurochem 138:60–73.

Li YC, Chanaday NL, Xu W, Kavalali ET (2017) Synaptotagmin-1- and synaptotagmin-7-dependent fusion mechanisms target synaptic vesicles to kinetically distinct endocytic pathways. Neuron 93:616–631.e3.

Mettlen M, Chen PH, Srinivasan S, Danuser G, Schmid SL (2018) Regulation of clathrin-mediated endocytosis. Annu Rev Biochem.

Moser T, Beutner D (2000) Kinetics of exocytosis and endocytosis at the cochlear inner hair cell afferent synapse of the mouse. Proc Natl Acad Sci U S A 97:883–888.

Nalefski EA, Falke JJ (1996) The C2 domain calcium-binding motif: structural and functional diversity. Protein Sci 5:2375–2390.

Neher E (2010) What is rate-limiting during sustained synaptic activity: vesicle supply or the availability of release sites. Front Synaptic Neurosci 2:144.

Neves G, Gomis A, Lagnado L (2001) Calcium influx selects the fast mode of endocytosis in the synaptic terminal of retinal bipolar cells. Proc Natl Acad Sci U S A 98:15282–15287.

Newton AC (2010) Protein kinase C: poised to signal. Am J Physiol Endocrinol Metab 298:E395–E402.

Nicholson-Tomishima K, Ryan TA (2004) Kinetic efficiency of endocytosis at mammalian CNS synapses requires synaptotagmin I. Proc Natl Acad Sci U S A 101:16648–16652.

Perrin BJ, Sonnemann KJ, Ervasti JM (2010) beta-actin and gamma-actin are each dispensable for auditory hair cell development but required for Stereocilia maintenance. PLoS Genet 6:e1001158.

Poskanzer KE, Fetter RD, Davis GW (2006) Discrete residues in the c(2)b domain of synaptotagmin I independently specify endocytic rate and synaptic vesicle size. Neuron 50:49–62.

Powell KA, Valova VA, Malladi CS, Jensen ON, Larsen MR, Robinson PJ (2000) Phosphorylation of dynamin I on ser-795 by protein kinase C blocks its association with phospholipids. J Biol Chem 275:11610–11617.

Renden R, von Gersdorff H (2007) Synaptic vesicle endocytosis at a CNS nerve terminal: faster kinetics at physiological temperatures and increased endocytotic capacity during maturation. J Neurophysiol 98:3349–3359.

Robinson PJ, Sontag JM, Liu JP, Fykse EM, Slaughter C, McMahon H, Südhof TC (1993) Dynamin GTPase regulated by protein kinase C phosphorylation in nerve terminals. Nature 365:163–166.

Sakaba T, Neher E (2001) Calmodulin mediates rapid recruitment of fast-releasing synaptic vesicles at a calyx-type synapse. Neuron 32:1119–1131.

Sankaranarayanan S, Ryan TA (2000) Real-time measurements of vesicle-SNARE recycling in synapses of the central nervous system. Nat Cell Biol 2:197–204.

Sankaranarayanan S, Ryan TA (2001) Calcium accelerates endocytosis of vSNAREs at hippocampal synapses. Nat Neurosci 4:129–136.

Shin W, Ge L, Arpino G, Villarreal SA, Hamid E, Liu H, Zhao WD, Wen PJ, Chiang HC, Wu LG (2018) Visualization of membrane pore in live cells reveals a dynamic-pore theory governing fusion and endocytosis. Cell 173:934–945.e12.

Smith C, Neher E (1997) Multiple forms of endocytosis in bovine adrenal chromaffin cells. J Cell Biol 139:885–894.

Soykan T, Kaempf N, Sakaba T, Vollweiter D, Goerdeler F, Puchkov D, Kononenko NL, Haucke V (2017) Synaptic vesicle endocytosis occurs on multiple timescales and is mediated by formin-dependent actin assembly. Neuron 93:854–866.e4.

Srinivasan G, Kim JH, von Gersdorff H (2008) The pool of fast releasing vesicles is augmented by myosin light chain kinase inhibition at the calyx of held synapse. J Neurophysiol 99:1810–1824.

Sun JY, Wu XS, Wu LG (2002) Single and multiple vesicle fusion induce different rates of endocytosis at a central synapse. Nature 417:555–559.

Sun T, Wu XS, Xu J, McNeil BD, Pang ZP, Yang W, Bai L, Qadri S, Molkentin JD, Yue DT, Wu LG (2010) The role of calcium/calmodulin-activated calcineurin in rapid and slow endocytosis at central synapses. J Neurosci 30:11838–11847.

Tan TC, Valova VA, Malladi CS, Graham ME, Berven LA, Jupp OJ, Hansra G, McClure SJ, Sarcevic B, Boadle RA, Larsen MR, Cousin MA, Robinson PJ (2003) Cdk5 is essential for synaptic vesicle endocytosis. Nat Cell Biol 5:701–710.

Thomas P, Lee AK, Wong JG, Almers W (1994) A triggered mechanism retrieves membrane in seconds after Ca^{2+}-stimulated exocytosis in single pituitary cells. J Cell Biol 124:667–675.

von Gersdorff H, Matthews G (1994) Inhibition of endocytosis by elevated internal calcium in a synaptic terminal. Nature 370:652–655.

Watanabe S, Rost BR, Camacho-Pérez M, Davis MW, Söhl-Kielczynski B, Rosenmund C, Jorgensen EM (2013) Ultrafast endocytosis at mouse hippocampal synapses. Nature 504:242–247.

Wu LG, Hamid E, Shin W, Chiang HC (2014) Exocytosis and endocytosis: modes, functions, and coupling mechanisms. Annu Rev Physiol 76:301–331.

Wu W, Wu LG (2007) Rapid bulk endocytosis and its kinetics of fission pore closure at a central synapse. Proc Natl Acad Sci U S A 104:10234–10239.

Wu W, Xu J, Wu XS, Wu LG (2005) Activity-dependent acceleration of endocytosis at a central synapse. J Neurosci 25:11676–11683.

Wu XS, Wu LG (2014) The yin and yang of calcium effects on synaptic vesicle endocytosis. J Neurosci 34:2652–2659.

Wu XS, McNeil BD, Xu J, Fan J, Xue L, Melicoff E, Adachi R, Bai L, Wu LG (2009) Ca(2+) and calmodulin initiate all forms of endocytosis during depolarization at a nerve terminal. Nat Neurosci 12:1003–1010.

Wu XS, Zhang Z, Zhao WD, Wang D, Luo F, Wu LG (2014) Calcineurin is universally involved in vesicle endocytosis at neuronal and nonneuronal secretory cells. Cell Rep 7:982–988.

Wu XS, Lee SH, Sheng J, Zhang Z, Zhao WD, Wang D, Jin Y, Charnay P, Ervasti JM, Wu LG (2016) Actin is crucial for all kinetically distinguishable forms of endocytosis at synapses. Neuron 92:1020–1035.

Wu Y, O'Toole ET, Girard M, Ritter B, Messa M, Liu X, McPherson PS, Ferguson SM, De Camilli P (2014) A dynamin 1-, dynamin 3- and clathrin-independent pathway of synaptic vesicle recycling mediated by bulk endocytosis. Elife 3:e01621.

Xia XM, Fakler B, Rivard A, Wayman G, Johnson-Pais T, Keen JE, Ishii T, Hirschberg B, Bond CT, Lutsenko S, Maylie J, Adelman JP (1998) Mechanism of calcium gating in small-conductance calcium-activated potassium channels. Nature 395:503–507.

Xu J, Wu LG (2005) The decrease in the presynaptic calcium current is a major cause of short-term depression at a calyx-type synapse. Neuron 46:633–645.

Yamashita T, Hige T, Takahashi T (2005) Vesicle endocytosis requires dynamin-dependent GTP hydrolysis at a fast CNS synapse. Science 307:124–127.

Yamashita T, Eguchi K, Saitoh N, von Gersdorff H, Takahashi T (2010) Developmental shift to a mechanism of synaptic vesicle endocytosis requiring nanodomain Ca2+. Nat Neurosci 13:838–844.

Yao J, Kwon SE, Gaffaney JD, Dunning FM, Chapman ER (2011) Uncoupling the roles of synaptotagmin I during endo- and exocytosis of synaptic vesicles. Nat Neurosci 15:243–249.

Yao L, Sakaba T (2012) Activity-dependent modulation of endocytosis by calmodulin at a large central synapse. Proc Natl Acad Sci U S A 109:291–296.

Yao LH, Rao Y, Varga K, Wang CY, Xiao P, Lindau M, Gong LW (2012) Synaptotagmin 1 is necessary for the Ca2+ dependence of clathrin-mediated endocytosis. J Neurosci 32:3778–3785.

Yue HY, Xu J (2014) Myosin light chain kinase accelerates vesicle endocytosis at the calyx of held synapse. J Neurosci 34:295–304.

Zhao WD, Hamid E, Shin W, Wen PJ, Krystofiak ES, Villarreal SA, Chiang HC, Kachar B, Wu LG (2016) Hemi-fused structure mediates and controls fusion and fission in live cells. Nature 534:548–552.

Zhu Y, Xu J, Heinemann SF (2009) Two pathways of synaptic vesicle retrieval revealed by single-vesicle imaging. Neuron 61:397–411.